Fast Fabrication of a Ag Nanostructure Substrate Using the Femtosecond Laser for Broad-Band and Tunable Plasmonic Enhancement

Ming Lun Tseng,[†,‡] Yao-Wei Huang,[†,‡] Min-Kai Hsiao,[§] Hsin Wei Huang,[†,‡] Hao Ming Chen,[†,⊥] Yu Lim Chen,[‡] Cheng Hung Chu,[†,‡] Nien-Nan Chu,[∥] You Je He,[‡] Chia Min Chang,[‡,¶] Wei Chih Lin,[‡] Ding-Wei Huang,[¶] Hai-Pang Chiang,[§,∥,#] Ru-Shi Liu,[⊥] Greg Sun,[△] and Din Ping Tsai[†,‡,∥,#,*]

[†]Graduate Institute of Applied Physics and [‡]Department of Physics, National Taiwan University, Taipei 106, Taiwan, [§]Institute of Optoelectronic Sciences, National Taiwan Ocean University, Keelung 202, Taiwan, [⊥]Department of Chemistry, National Taiwan University, Taipei 106, Taiwan, [∥]Instrument Technology Research Center, National Applied Research Laboratories, Hsinchu 300, Taiwan, [¶]Institute of Photonics and Optoelectronics, National Taiwan University, Taipei 106, Taiwan, [#]Research Center for Applied Sciences, Academia Sinica, Taipei 115, Taiwan, and [△]Department of Physics, University of Massachusetts, Boston, Massachusetts 02125, United States

ABSTRACT

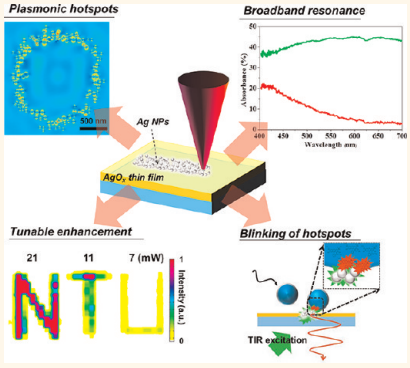

Using a femtosecond laser, we have transformed the laser-direct-writing technique into a highly efficient method that can process AgO_x thin films into Ag nanostructures at a fast scanning rate of 2000 μm^2/min. The processed AgO_x thin films exhibit broad-band enhancement of optical absorption and effectively function as active SERS substrates. Probing of the plasmonic hotspots with dyed polymer beads indicates that these hotspots are uniformly distributed over the treated area.

KEYWORDS: plasmonics · laser-direct-writing technique · hotspot · fluorescence enhancement · SERS

Metal nanoparticles (NPs) have attracted much attention in recent years because of the strongly localized electric fields induced by the collective oscillation of free electrons in the metal that interact with the light impinging on the NPs. This phenomenon is called localized surface plasmon resonance (LSPR),[1−4] which is known to strongly depend on the size, shape, surrounding medium, and separation of NPs.[2−10] LSPR can effectively harvest the electromagnetic energy of incoming light and concentrate it into the "plasmonic hotspots".[11−14] Enhancement of local-field intensity on the order of 10^6 can be obtained relative to that of incident light.[15−17]

The phenomenon of hotspots has been successfully employed in surface-enhanced Raman spectroscopy (SERS) for molecular sensing,[18−25] in photovoltaics,[26−28] and in photocatalytic water splitting,[29,30] in addition to a number of other potential applications such as medical imaging and cancer treatment.[31,32] It has also led to the demonstration of plasmonic nanolasers.[33,34] Many of these applications require active substrates consisting of metal nanostructures capable of delivering a high density of hotspots. A number of techniques have been developed to accomplish this purpose. For example, focused ion beam[35] and e-beam[23] have been used to fabricate plasmonic subwavelength structures with well-defined geometries. These lithographic methods capable of treating very limited substrate area with a long processing time also require expensive setup and a highly stable environment. In comparison, the relatively inexpensive nanosphere lithography[36] can be employed on large-scale substrates, but uniformity has been a significant challenge. Laser ablation is another interesting technique where metal NPs are lifted off from a piece of metal submerged in a solvent with a laser beam,[37,38] but the NPs always end up

* Address correspondence to dptsai@phys.ntu.edu.tw.

Received for review March 2, 2012 and accepted April 28, 2012.

Published online April 28, 2012
10.1021/nn300947n

© 2012 American Chemical Society

in a solvent. An efficient, cost-effective technique capable of rapidly treating large-area substrates with good uniformity, high throughput, and better flexibility is obviously desirable. Among the various fabrication methods, the laser-direct-writing (LDW) technique is one of the best candidates for the rapid, low-cost processing of micro- and nanostructures.[39−43] This low-cost technique has the potential to achieve throughput of 2−5 orders of magnitude higher than other maskless techniques.[43,44] In optical data storage systems, 4×10^{10} nanofeatures of 20 nm in diameter can be written by a laser beam in an optical disk driver in 30 min on a single-sided commercial DVD disk (surface area ~100 cm^2) coated with the data recording medium AgInSbTe alloy.[44] While this writing speed may not be matched any time soon by any of the plasmonic substrate fabrication techniques, it does inspire the effort to explore the LDW technique on mediums that can be rapidly processed into plasmonic nanostructures. AgO_x is such a medium from which Ag nanostructures with dense hotspots can be obtained by the LDW method following the photoreduction reaction that produces an aggregate of Ag NPs from AgO_x film *in situ* as[45,46]

$$2AgO_x \xrightarrow{h\nu} 2Ag + xO_2 \qquad (1)$$

In this paper, we report fabrication of Ag NPs from a AgO_x thin film deposited on a glass substrate with the LDW technique using a femtosecond laser. Different from LDW methods that use either continuous or nanosecond lasers, the illumination of a femtosecond laser turns out to be far more efficient in processing AgO_x thin films into aggregates of Ag NPs in terms of both processing speed and sample performance. The aggregates of Ag NPs are generated on the laser-illuminated spot, which exhibits a broad-band optical response in the visible regime. In order to directly probe the hotspots around the Ag NPs under the illumination of a white light source, we have used dyed polymer beads that randomly drift in a water solution. As the beads come close to the hotspots, the dye molecules embedded in the beads get excited and subsequently relax by emitting light. In this work, we chose to use dyed polymer beads instead of dye molecules because the latter cannot be easily removed from the sample surface, making it not reusable for subsequent measurement. The experimental setup for fabrication of Ag NPs and detection of hotspots is illustrated in Figure 1. The processed sample is mounted on a total internal reflection (TIR) microscope and submerged in a water solution of dyed polymer beads. A charge-coupled device (CCD) camera is used to record the fluorescence from the dye molecules at the hotspots. A series of blinking has been observed as the dye molecule carrying beads move in and out of the hotspots.

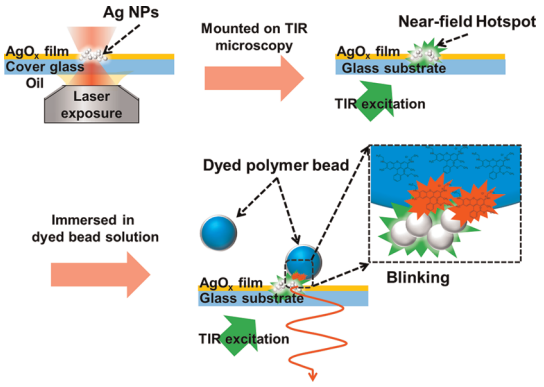

Figure 1. Schematics of LDW processing AgO_x thin film being mounted on a TIR microscope, immersed in dyed polymer bead solution, excitation of drifting beads at hotspots, and blinking of dye molecules embedded in the beads.

To demonstrate that the processed femtosecond laser-treated AgO_x thin films can be effectively used as plasmonic substrates, we have also carried out SERS measurement. We find that the laser-treated AgO_x thin film indeed acts as a SERS-active substrate and the enhancement is comparable to the other previously studied SERS substrates.[22] The processing technique is not only faster but also far simpler than other reported methods.[35,36] In addition, the hotspots are found to be uniformly distributed across the laser-treated AgO_x area. SERS intensity can also be easily controlled by varying the laser treatment condition.

RESULTS AND DISCUSSION

A matrix of "rings" is made on the 15 nm thick AgO_x film by a femtosecond laser (λ = 800 nm, pulse duration = 140 fs, repetition rate = 80 MHz; see Methods section). The power of the laser beam is 14 mW. Each ring is created by a single laser shot with the exposure time of 30 ms. The optical reflection image in Figure 2a clearly reveals the ring structures that are formed under the illumination of a laser beam with inner and outer diameters of roughly 0.5 and 1.4 μm, respectively. The rings are made of Ag structures as evidenced by their higher reflectivity. The AFM image in Figure 2b suggests that inner ring regions are ablated holes, showing as dark purple spots in the reflectivity measurement. Outside of the ring, the AgO_x layer remains intact. There is a transition region where Ag NPs are formed sitting on AgO_x with different layer thickness. Figure 2c is the magnified SEM image of a single ring where the aggregate of disordered Ag NPs is shown as bright spots. The Ag NPs are also characterized by a high-resolution transmission electron microscope (TEM). The lattice fringes with *d* spacing of 0.235 nm match the interspacing of the (111) planes of the face-centered cubic Ag, which is also in agreement with that of bulk Ag (Figure 2d). The selected electron diffraction pattern (inset of Figure 2d) shows the polycrystalline characteristic.

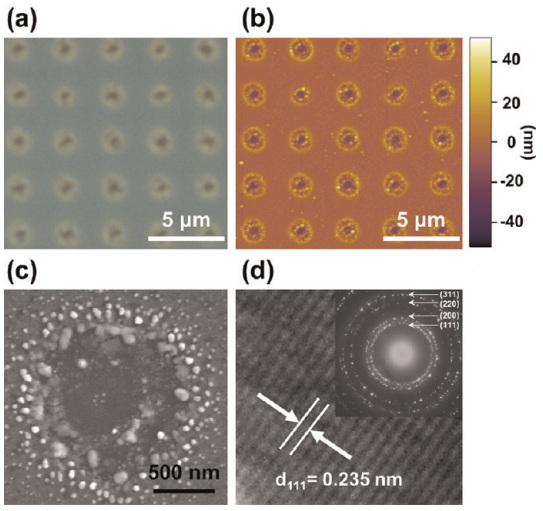

Figure 2. (a) Optical reflection and (b) AFM image of the aggregates of Ag nanoparticles obtained on the laser-illuminated AgO_x thin film. (c) Magnified SEM image of an aggregate of Ag NPs. (d) TEM image and electron diffraction pattern of laser-generated Ag NPs.

Broad-Band Resonant Light Absorption of Laser-Generated Ag Structures. Figure 3a shows the size distribution of generated Ag NPs in Figure 2d, which varies from 10 to 100 nm in diameter with an average size of 32.2 nm. In addition, the SEM analysis reveals that the Ag NP aggregate possesses a fractal structure with the characteristic dimension of $D \simeq 1.75$, similar to the fractal Ag NP aggregates made by chemical reduction methods.[14,47] Figure 3b shows the absorption spectra of the AgO_x thin film before and after laser processing. The relatively strong absorption around 400 nm for the unprocessed AgO_x is due to the existence of metallic Ag in the film.[46] The laser-treated AgO_x thin film exhibits significant increase of absorption in the wavelength range of 400−700 nm. The optical absorption spectrum is much broader than those obtained from photoreduced Ag structures generated by pulsed lasers with longer pulse durations (nanoseconds to milliseconds), which typically display an absorption peak around 430 nm as a result of the LSPR mode of individual Ag monomers.[47−50]

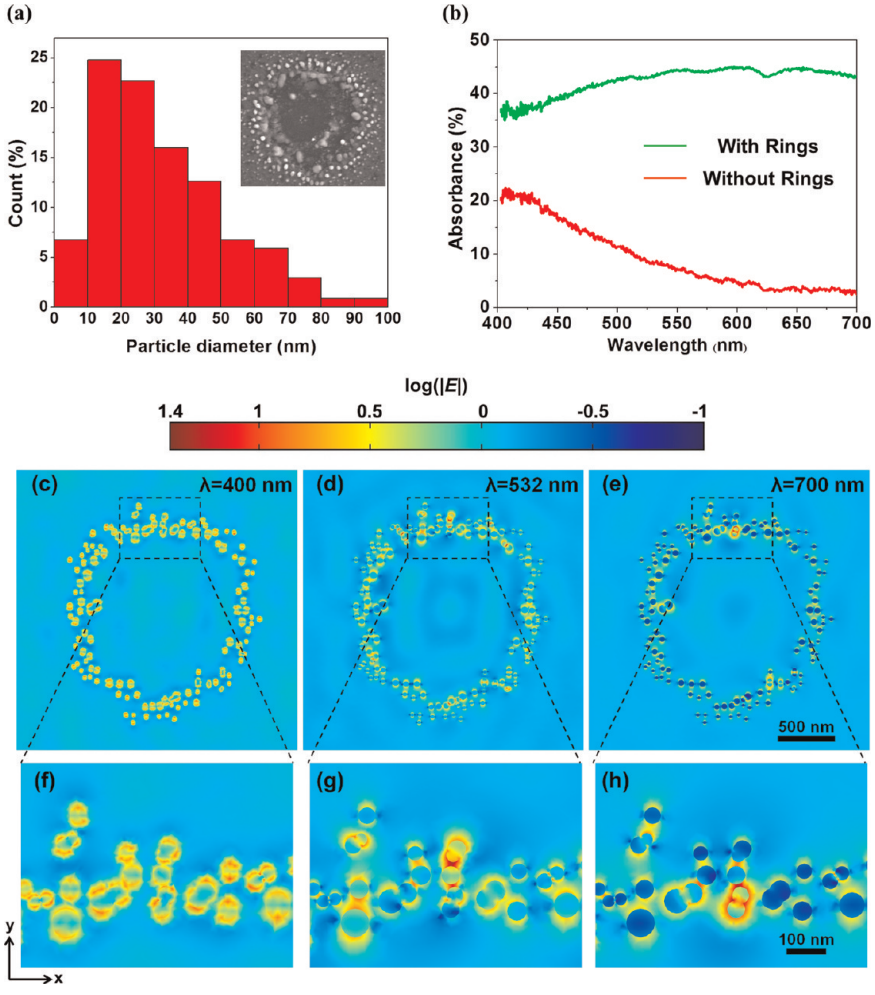

Figure 3. (a) Histogram of Ag NP diameters. (b) Optical absorption spectra collected from laser-processed as well as untreated areas. (c−h) FEM electromagnetic simulation results of Ag NP aggregates obtained with normal incident *y*-polarized laser light at wavelengths of 400, 532, and 700 nm.

We have also carried out the electromagnetic (EM) intensity simulation using a full-wave three-dimensional Maxwell equation solver (COMSOL Multiphysics 3.5a) based on the finite element method (FEM). The Ag NPs in Figure 2d are chosen with the use of image processing software. The Ag NPs are on a BK-7 glass substrate (refractive index = 1.46) in the simulation. The permittivity of Ag is described by the Drude–Lorentz model[51] with size effect taken into consideration.[52] Three incident wavelengths of 400, 532, and 700 nm that are *y*-polarized (axis shown in Figure 3) are launched along the negative *z*-direction. Overall, the best enhancement of electric field intensity reaches 1000 relative to that of incident light. The simulated results in Figure 3c,f show that the hotspots are dominated by the LSPR of individual Ag NPs rather than by the coupling between the NPs as incident light at $\lambda = 400$ nm gets absorbed by the nanostructure. At $\lambda = 532$ nm (Figure 3d,g) and 700 nm (Figure 3e,h), however, the hotspots are localized in the narrow gaps of neighboring NPs, suggesting strong coupling between them. Upon examination of Figure 3g,h, it is not difficult to see that the locations of hotspots have changed as the incident wavelength changes. There is reason to believe that, in a highly disordered system of NPs such as this, the EM energy of different wavelength within the broad spectrum of an incident light can get concentrated onto different locations of the Ag NP aggregates, resulting in enhancement of absorption over a wide spectral range across the entire dimension of the rings. This broad absorption enhancement covering the entire visible spectral range is obviously desirable for harvesting solar energy into plasmonically enhanced solar cells. Atwater *et al.* recently proposed a solar energy absorber based on a plasmonic nanostructure consisting of a metal–insulator–metal three-layer system.[53] The total thickness of their three layers is 260 nm, about 17 times as thick as the AgO_x thin film (15 nm) used in this work. The fabrication of their solar nanostructure required e-beam lithography with a bilayer photoresist process on top of multilayer deposition involving thermal evaporation and chemical vapor deposition. In comparison, the fabrication technique presented in this work is much faster, simpler, and less expensive, and the laser-treated AgO_x thin films show potential to be optimized as an efficient and low-cost solar energy absorber.

Blinking Experiment. The laser-treated AgO_x thin film is mounted in a total internal reflection microscope (TIRM) system, which is based on an Olympus IX-70 microscope and a Nd:YAG laser (532 nm). A high numerical aperture oil-immersed objective (Olympus Co., Plan-Apo Oil TIRFM, 60×, NA = 1.45) is used, and the incident angle is controlled by a fiber illuminator. The reflection of the laser beam is blocked, and the dark-field images are recorded by a CCD camera (Hamamatsu Corp., ORCA-ER). The intensity is carefully adjusted by neutral density filters (Thorlabs Inc., NDC-100C-2M) to yield about 1.26 μW immediately before the sample. The upper surface of film is totally immersed in the suspension of dyed polymer beads (Duke Scientific Co., R500 fluorescent polymer spheres) (diameter of 500 nm, refractive index of 1.59, 542 nm ex/612 nm fl). The dyed beads are uniformly dispersed throughout the deionized water (Milipore), and the concentration is set at 5×10^{-5} M.

As soon as the solution is dropped on the sample, blinking can be observed and recorded (see video in Supporting Information). A frame of the acquired original video is shown in Figure 4a; the size of the recorded area is around $70 \times 75\ \mu m^2$, and the camera's exposure time is 0.2 s. Many blinking spots can be observed at the laser-generated Ag rings simultaneously. In the 200 s observation period, 817 blinking events are recorded, while no obvious blinking spots are observed on a clean glass substrate (we use glass substrate in the control experiment because we consider that the Ag NPs can be formed on the AgO_x thin film with a long illumination time of a 532 nm laser) in a control experiment.

We also simulated the near-field interaction between the dyed polymer bead and Ag NPs using a three-dimensional FEM model. The simulation is conducted on two real Ag NPs, one with a diameter of 44 nm and another of 50 nm, and both are captured in SEM images. As illustrated in Figure 4b, a polymer bead with dye molecules (500 nm in diameter, refractive index of 1.59) is separated 10 nm from the two Ag NPs sitting on the glass substrate. A TM-polarized light at 532 nm is incident at an angle of 66°, traveling from the BK-7 glass to the water solution. Results shown in Figure 4c clearly demonstrate the localization of EM field that is enhanced by a factor of 1000 in the vicinity of Ag NPs under the illumination of a linear TM-polarized light.

The enhanced fluorescence of dye molecules on polymer beads is a result of their near-field coupling with the LSPR modes of Ag NPs. The enhancement takes place in two sequential steps, one during the optical absorption where the strong fields in hotspots enhance the in-coupling of energy into the dye molecules, the other during the relaxation of the molecules in which the energy absorbed in the previous stage emits into the LSPR modes at rates that are enhanced by the Purcell factors associated with the large density of states of the LSPR modes that are coupled with the far field.[54]

Surface-Enhanced Raman Spectroscopy. Raman spectroscopy is an effective method for identifying molecules through their vibrational signatures.[55–57] SERS as a technique that significantly improved the Raman process has led to its wide applications in studying molecular properties of low concentrations and in some cases with sensitivity down to the level of a single molecule.[18,19]

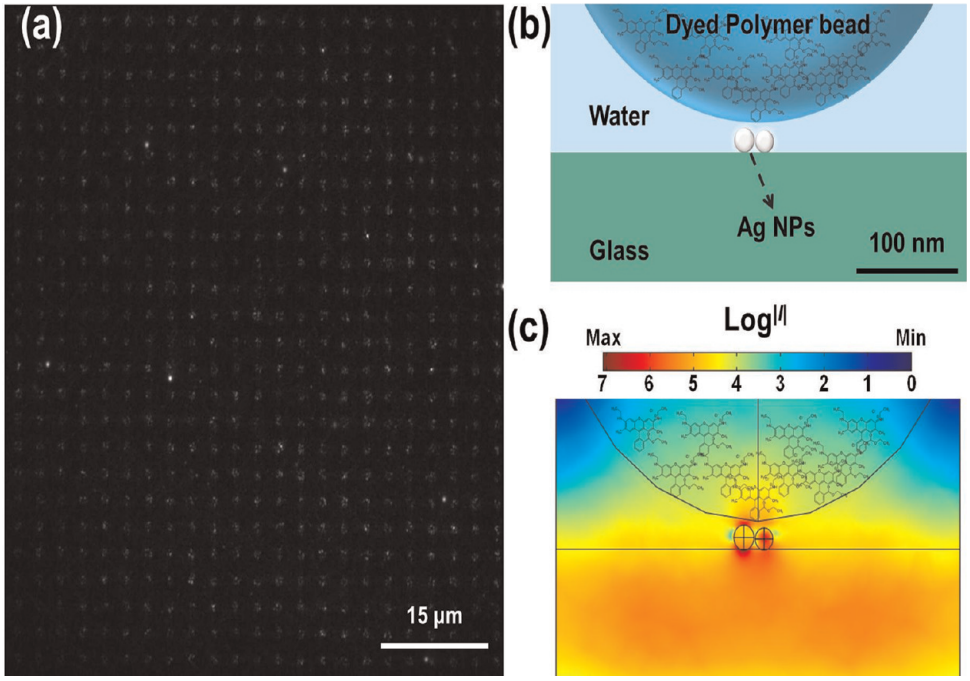

Figure 4. (a) Screenshot of the original video recording of the blinking of dyed polymer beads (Supporting Information). (b) Illustration of a uniformly dyed polymer bead of 500 nm in diameter in close proximity of a Ag NP pair of about 50 nm in diameter. (c) FEM electromagnetic intensity simulation of a dyed polymer bead on Ag NPs. A TM-polarized light of 532 nm is incident onto the glass substrate with an incident angle of 66°.

To demonstrate the effectiveness of the laser-treated AgO_x as a substrate for Raman measurement, we used the LDW technique to create the "NTU" pattern on its surface. Each letter consists of an aggregate of Ag NPs. The three letters are written at different laser powers of 21, 11, and 7 mW, respectively. The well-known Rhodamine 6G (R6G) dye molecules adsorbed at the laser-treated AgO_x thin film are employed to probe the local electric field enhancement. R6G solution in 10^{-5} M is pipetted on the treated AgO_x thin film and purged by pure N_2 gas. The sample is then analyzed by a scanning confocal Raman microscope (WITec, CMR200) equipped with a semiconductor laser (λ = 532 nm) as the light source.

Figure 5a,b shows the Raman and optical reflection images collected from the same LDW-generated pattern "NTU". As shown in Figure 5a, the SERS signal from the laser-treated regions is obviously brighter than that of the bare untreated region. In addition, the Raman signal varies from letter to letter and displays strongest intensity on the letter N written with the highest laser power (21 mW), indicating different levels of enhancement. Next, we use AFM measurement to establish the relationship between the SERS enhancement and the processing power. The AFM image in Figure 5c shows the surface morphology of each character which increases in width and depth as the processing laser power. The magnified AFM images in Figure 5e–g reveal that the average size of Ag NPs decreases, while the surface density (NP number/μm^2) increases with laser power. Since different surface densities of Ag NPs with various configurations and spacing widths usually lead to varying intensities of local enhancement because hotspots are likely to be generated in the gaps between metal NPs,[12,18] we can then use laser power to control the field intensities of the hotspots which in turn will allow for performance optimization.

These results indicate that the laser-treated AgO_x thin films can indeed be used for SERS measurement. In addition, the fabrication technique developed in this work can be used to rapidly and reliably produce large-area SERS-active substrates. The AFM, optical reflection, and Raman images in Figure S-1 of Supporting Information are collected from the Ag NP aggregate over an area of 65 × 100 μm^2 obtained by scanning the femtosecond laser beam with the output power of 14 mW across the AgO_x thin film at the scanning speed of around 33.3 μm/s for the scanning width of 1 μm, yielding an area processing rate of about 2000 μm^2/min. The AFM measurement shows the similar Ag NP aggregate. Figure 5d shows the Raman spectra of R6G measured at the positions on the AgO_x thin film with and without laser processing. Within the laser-treated region (red line of Figure 5d), typical features of R6G at 612, 770, 1188, 1357, and 1646 cm^{-1} can be identified,[22] in contrast to the Raman signal at the region without laser processing (green line in Figure 5d), which showed no such features at all. Using the protocol in ref 25, we have determined the Raman enhancement factor of 1.15 × 10^8. In comparison with the nanosphere lithographic technique[22,36] often used to fabricate plasmonic substrates, the LDW technique

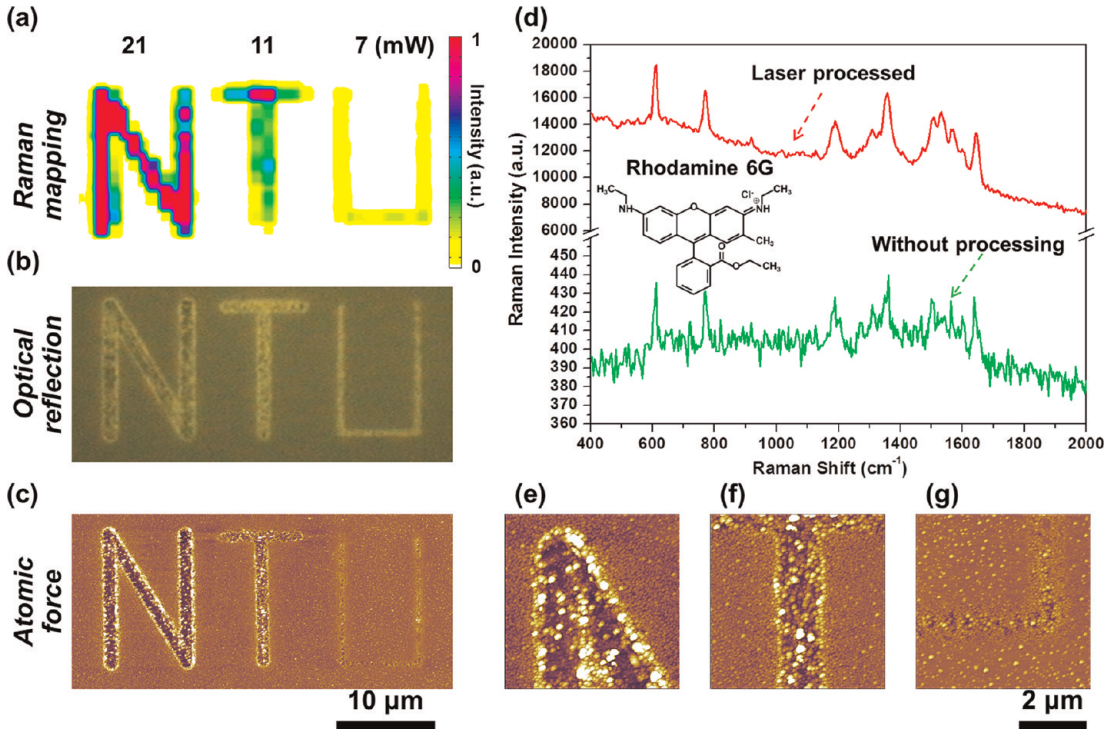

Figure 5. (a–c) Raman, optical reflection, AFM images of "NTU" pattern written on AgO_x thin film by the femtosecond laser. Letter "N" is written with a laser power of 21 mW, "T" with 11 mW, and "U" with 7 mW. The Raman image is obtained from R6G (10^{-5} M) adsorbed on the laser-patterned AgO_x thin film by integrating the spectral intensity over their identified Raman peaks ranging from 568 to 623 cm^{-1}. (d) SERS spectra of R6G molecules on the AgO_x thin films with and without laser processing (the corresponding Raman image is shown in Figure S-1 of Supporting Information.) (e–g) Magnified AFM images of the letters N, T, and U shown on the scale.

employed here not only resulted in comparable Raman enhancement but also yielded more dense hotspots that are uniformly distributed across the treated area on AgO_x thin film. This technique is also found to be more efficient when compared to other laser illuminating methods involving either continuous[58] or nanosecond[49] lasers. With the much higher pulse power delivered by the femtosecond laser, we were able to continuously scan across the sample surface at the rate of 2000 μm^2 per minute, which is far more efficient than the typical illumination time of a few minutes required on a single spot of 1 μm^2 by those other methods. This highly improved technique should broaden the use of laser-treated AgO_x thin films for plasmonic applications.

CONCLUSION

Using LDW technique with a femtosecond laser, we have demonstrated its effectiveness in processing a AgO_x thin film deposited on a glass substrate into Ag nanostructures consisting of aggregates of Ag NPs. This technique has the advantage of rapidly processing large-area substrates at low costs over other reported processing methods. Broad-band optical absorption enhancement in the visible region has been measured from the processed AgO_x thin films, suggesting its potential application in harvesting solar energy. Blinking of dyed polymer beads has been observed as they move in and out of the plasmonic hotspots around the Ag NPs in a water solution. The LDW-treated AgO_x thin film can also be utilized as an active substrate for SERS measurement. We have successfully used the LDW technique to create patterns on a substrate with different levels of Raman enhancement by varying the laser power. The femtosecond LDW technique has been proven as a flexible and versatile method for processing large-area AgO_x thin films into plasmonically active substrates. It holds promise as a highly efficient and cost-effective approach for applications in solar energy harvesting, molecular sensing, plasmonic photocatalyst, and plasmonic nanolasers.

METHODS

The 15 nm thick AgO_x thin films are reactively sputtered on a transparent BK7 glass (Matsunami cover glass, 0.15 mm thickness) in an Ar/O_2 (gas ratio 10/25) mixed-gas atmosphere by a conventional magnetron sputtering machine (Shibaura Mechatronics Corp.). The as-deposited AgO_x thin film is mounted on a nanoscale precision stage (Mad City Lab. Inc., Nano-LP200) as shown in Figure S-2 of Supporting Information. A Ti:sapphire femtosecond laser (Coherent Inc., λ = 800 nm, pulse duration = 140 fs, repetition rate = 80 MHz) is used as a light source. An attenuator and a shutter are used for the control of the laser power and exposure time, respectively. The laser

beam is expanded to a diameter of 6 mm by a spatial filter. A $\lambda/4$ waveplate transforms the laser beam into circular polarization. Finally, the laser beam is focused by a high numerical aperture oil-immersion objective lens (Zeiss, Plan-Apochromat, 100×, 1.4 NA, 0.17 mm working distance) through the transparent substrate on the AgO_x thin film. A CCD camera is used for real-time monitoring. Characterization of laser-structured AgO_x thin film is carried out using an AFM (Asylum Research, MFP-3D), optical microscope (Leica, MPV-SP, 100×, 0.9 NA), and scanning electron microscope (SEM, HITACHI, S-4300). The total absorbance of the sample is measured over a wavelength range of 400−700 nm using an optical spectrometer (B&W Tek Inc., BTC111E CCD array spectrometer).

Conflict of Interest: The authors declare no competing financial interest.

Acknowledgment. The authors acknowledge financial support from National Science Council, Taiwan, under Grant Nos. 99-2120-M-002-012, 99-2911-I-002-127, 100-2120-M-002-008, and 100-2923-M-002-007-MY3. They are also grateful to National Center for Theoretical Sciences, Taipei Office, Molecular Imaging Center of National Taiwan University and National Center for High-Performance Computing, Taiwan, for their support. G.S. acknowledges partial support from U.S. Air Force Office of Scientific Research (FA9550-10-1-0417).

Supporting Information Available: The femtosecond laser system; video of blinking experiment; laser-treated AgO_x thin film for large-scale SERS substrate. This material is available free of charge *via* the Internet at http://pubs.acs.org.

REFERENCES AND NOTES

1. Hafner, J. H.; Nordlander, P.; Weiss, P. S. Virtual Issue on Plasmonics. *ACS Nano* **2011**, *5*, 4245–4248.
2. Zuloaga, J.; Prodan, E.; Nordlander, P. Quantum Plasmonics: Optical Properties and Tunability of Metallic Nanorods. *ACS Nano* **2010**, *4*, 5269–5276.
3. Nordlander, P.; Le, F. Plasmonic Structure and Electromagnetic Field Enhancements in the Metallic Nanoparticle-Film System. *Appl. Phys. B: Lasers Opt.* **2006**, *84*, 35–41.
4. Murray, W. A.; Barnes, W. L. Plasmonic Materials. *Adv. Mater.* **2007**, *19*, 3771–3782.
5. Knight, M. W.; Wu, Y. P.; Lassiter, J. B.; Nordlander, P.; Halas, N. J. Substrates Matter: Influence of an Adjacent Dielectric on an Individual Plasmonic Nanoparticle. *Nano Lett.* **2009**, *9*, 2188–2192.
6. Prodan, E.; Radloff, C.; Halas, N. J.; Nordlander, P. A Hybridization Model for the Plasmon Response of Complex Nanostructures. *Science* **2003**, *302*, 419–422.
7. Hao, F.; Sonnefraud, Y.; Van Dorpe, P.; Maier, S. A.; Halas, N. J.; Nordlander, P. Symmetry Breaking in Plasmonic Nanocavities: Subradiant LSPR Sensing and a Tunable Fano Resonance. *Nano Lett.* **2008**, *8*, 3983–3988.
8. Nordlander, P. The Ring: A Leitmotif in Plasmonics. *ACS Nano* **2009**, *3*, 488–492.
9. Brown, L. V.; Sobhani, H.; Lassiter, J. B.; Nordlander, P.; Halas, N. J. Heterodimers: Plasmonic Properties of Mismatched Nanoparticle Pairs. *ACS Nano* **2010**, *4*, 819–832.
10. Slaughter, L. S.; Wu, Y. P.; Willingham, B. A.; Nordlander, P.; Link, S. Effects of Symmetry Breaking and Conductive Contact on the Plasmon Coupling in Gold Nanorod Dimers. *ACS Nano* **2010**, *4*, 4657–4666.
11. Shalaev, V. M.; Markel, V. A.; Poliakov, E. Y.; Armstrong, R. L.; Safonov, V. P.; Sarychev, A. K. Nonlinear Optical Phenomena in Nanostructured Fractal Materials. *J. Nonlinear Opt. Phys. Mater.* **1998**, *7*, 131–152.
12. Weber, M. L.; Willets, K. A. Correlated Super-Resolution Optical and Structural Studies of Surface-Enhanced Raman Scattering Hot Spots in Silver Colloid Aggregates. *J. Phys. Chem. Lett.* **2011**, *2*, 1766–1770.
13. Le, F.; Brandl, D. W.; Urzhumov, Y. A.; Wang, H.; Kundu, J.; Halas, N. J.; Aizpurua, J.; Nordlander, P. Metallic Nanoparticle Arrays: A Common Substrate for Both Surface-Enhanced Raman Scattering and Surface-Enhanced Infrared Absorption. *ACS Nano* **2008**, *2*, 707–718.
14. Tsai, D. P.; Kovacs, J.; Wang, Z. H.; Moskovits, M.; Shalaev, V. M.; Suh, J. S.; Botet, R. Photon Scanning-Tunneling-Microscopy Images of Optical-Excitations of Fractal Metal Colloid Clusters. *Phys. Rev. Lett.* **1994**, *72*, 4149–4152.
15. Li, K. R.; Stockman, M. I.; Bergman, D. J. Self-Similar Chain of Metal Nanospheres as an Efficient Nanolens. *Phys. Rev. Lett.* **2003**, *91*, 227402.
16. Hao, E.; Schatz, G. C. Electromagnetic Fields around Silver Nanoparticles and Dimers. *J. Chem. Phys.* **2004**, *120*, 357–366.
17. Schatz, G. C.; Young, M. A.; Van Duyne, R. P. Electromagnetic Mechanism of SERS. *Top. Appl. Phys.* **2006**, *103*, 19–46.
18. Talley, C. E.; Jackson, J. B.; Oubre, C.; Grady, N. K.; Hollars, C. W.; Lane, S. M.; Huser, T. R.; Nordlander, P.; Halas, N. J. Surface-Enhanced Raman Scattering from Individual Au Nanoparticles and Nanoparticle Dimer Substrates. *Nano Lett.* **2005**, *5*, 1569–1574.
19. Nie, S. M.; Emory, S. R. Probing Single Molecules and Single Nanoparticles by Surface-Enhanced Raman Scattering. *Science* **1997**, *275*, 1102–1106.
20. Dawson, P.; Duenas, J. A.; Boyle, M. G.; Doherty, M. D.; Bell, S. E. J.; Kern, A. M.; Martin, O. J. F.; Teh, A. S.; Teo, K. B. K.; Milne, W. I. Combined Antenna and Localized Plasmon Resonance in Raman Scattering from Random Arrays of Silver-Coated, Vertically Aligned Multiwalled Carbon Nanotubes. *Nano Lett.* **2011**, *11*, 365–371.
21. Strelau, K. K.; Schüler, T.; Möller, R.; Fritzsche, W.; Popp, J. Novel Bottom-Up SERS Substrates for Quantitative and Parallelized Analytics. *ChemPhysChem* **2009**, *11*, 394–398.
22. Lin, W. C.; Huang, S. H.; Chen, C. L.; Chen, C. C.; Tsai, D. P.; Chiang, H. P. Controlling SERS Intensity by Tuning the Size and Height of a Silver Nanoparticle Array. *Appl. Phys. A: Mater. Sci. Process.* **2010**, *101*, 185–189.
23. Duan, H.; Hu, H.; Kumar, K.; Shen, Z.; Yang, J. K. W. Direct and Reliable Patterning of Plasmonic Nanostructures with Sub-10-nm Gaps. *ACS Nano* **2011**, *5*, 7593–7600.
24. Banaee, M. G.; Crozier, K. B. Mixed Dimer Double-Resonance Substrates for Surface-Enhanced Raman Spectroscopy. *ACS Nano* **2011**, *5*, 307–314.
25. Willets, K. A.; Van Duyne, R. P. Localized Surface Plasmon Resonance Spectroscopy and Sensing. *Annu. Rev. Phys. Chem.* **2007**, *58*, 267–297.
26. Pillai, S.; Catchpole, K. R.; Trupke, T.; Green, M. A. Surface Plasmon Enhanced Silicon Solar Cells. *J. Appl. Phys.* **2007**, *101*, 093105.
27. Ferry, V. E.; Polman, A.; Atwater, H. A. Modeling Light Trapping in Nanostructured Solar Cells. *ACS Nano* **2011**, *5*, 10055–10064.
28. Wu, J. L.; Chen, F. C.; Hsiao, Y. S.; Chien, F. C.; Chen, P. L.; Kuo, C. H.; Huang, M. H.; Hsu, C. S. Surface Plasmonic Effects of Metallic Nanoparticles on the Performance of Polymer Bulk Heterojunction Solar Cells. *ACS Nano* **2011**, *5*, 959–967.
29. Silva, C. G.; Juarez, R.; Marino, T.; Molinari, R.; Garcia, H. Influence of Excitation Wavelength (UV or Visible Light) on the Photocatalytic Activity of Titania Containing Gold Nanoparticles for the Generation of Hydrogen or Oxygen from Water. *J. Am. Chem. Soc.* **2011**, *133*, 595–602.
30. Gao, H. W.; Liu, C.; Jeong, H. E.; Yang, P. D. Plasmon-Enhanced Photocatalytic Activity of Iron Oxide on Gold Nanopillars. *ACS Nano* **2012**, *6*, 234–240.
31. Bardhan, R.; Lal, S.; Joshi, A.; Halas, N. J. Theranostic Nanoshells: From Probe Design to Imaging and Treatment of Cancer. *Acc. Chem. Res.* **2011**, *44*, 936–946.
32. Loo, C.; Lowery, A.; Halas, N. J.; West, J.; Drezek, R. Immunotargeted Nanoshells for Integrated Cancer Imaging and Therapy. *Nano Lett.* **2005**, *5*, 709–711.
33. Noginov, M. A.; Zhu, G.; Belgrave, A. M.; Bakker, R.; Shalaev, V. M.; Narimanov, E. E.; Stout, S.; Herz, E.; Suteewong, T.; Wiesner, U. Demonstration of a Spaser-Based Nanolaser. *Nature* **2009**, *460*, 1110–1113.
34. Bergman, D. J.; Stockman, M. I. Surface Plasmon Amplification by Stimulated Emission of Radiation: Quantum

Generation of Coherent Surface Plasmons in Nanosystems. *Phys. Rev. Lett.* **2003**, *90*, 027402–027405.
35. Kim, S.; Jin, J. H.; Kim, Y. J.; Park, I. Y.; Kim, Y.; Kim, S. W. High-Harmonic Generation by Resonant Plasmon Field Enhancement. *Nature* **2008**, *453*, 757–760.
36. Haynes, C. L.; Young, M. A.; Van Duyne, R. P. Nanosphere Lithography: A Versatile Nanofabrication Tool for Studies of Size-Dependent Nanoparticle Optics. *J. Phys. Chem. B* **2001**, *105*, 5599–5611.
37. Mafune, F.; Kohno, J.; Takeda, Y.; Kondow, T.; Sawabe, H. Formation and Size Control of Sliver Nanoparticles by Laser Ablation in Aqueous Solution. *J. Phys. Chem. B* **2000**, *104*, 9111–9117.
38. Tsuji, T.; Kakita, T.; Tsuji, M. Preparation of Nano-Size Particles of Silver with Femtosecond Laser Ablation in Water. *Appl. Surf. Sci.* **2003**, *206*, 314–320.
39. Chen, Z. C.; Hong, M. H.; Lim, C. S.; Han, N. R.; Shi, L. P.; Chong, T. C. Parallel Laser Microfabrication of Large-Area Asymmetric Split Ring Resonator Metamaterials and its Structural Tuning for Terahertz Resonance. *Appl. Phys. Lett.* **2010**, *96*, 181101.
40. Han, N. R.; Chen, Z. C.; Lim, C. S.; Ng, B.; Hong, M. H. Broadband Multi-Layer Terahertz Metamaterials Fabrication and Characterization on Flexible Substrates. *Opt. Express* **2011**, *19*, 6990–6998.
41. Tseng, M. L.; Chen, B. H.; Chu, C. H.; Chang, C. M.; Lin, W. C.; Chu, N. N.; Mansuripur, M.; Liu, A. Q.; Tsai, D. P. Fabrication of Phase-Change Chalcogenide $Ge_2Sb_2Te_5$ Patterns by Laser-Induced Forward Transfer. *Opt. Express* **2011**, *19*, 16975–16984.
42. Kuznetsov, A. I.; Evlyukhin, A. B.; Goncalves, M. R.; Reinhardt, C.; Koroleva, A.; Arnedillo, M. L.; Kiyan, R.; Marti, O.; Chichkov, B. N. Laser Fabrication of Large-Scale Nanoparticle Arrays for Sensing Applications. *ACS Nano* **2011**, *5*, 4843–4849.
43. Srituravanich, W.; Pan, L.; Wang, Y.; Sun, C.; Bogy, D. B.; Zhang, X. Flying Plasmonic Lens in the Near Field for High-Speed Nanolithography. *Nat. Nanotechnol.* **2008**, *3*, 733–737.
44. Lin, S. K.; Lin, I. C.; Tsai, D. P. Characterization of Nano Recorded Marks at Different Writing Strategies on Phase-Change Recording Layer of Optical Disks. *Opt. Express* **2006**, *14*, 4452–4458.
45. Ho, F. H.; Chang, H. H.; Lin, Y. H.; Chen, B. M.; Wang, S. Y.; Tsai, D. P. Functional Structures of AgO_x Thin Film for Near-Field Recording. *Jpn. J. Appl. Phys.* **2003**, *42*, 1000–1004.
46. Liu, W. C.; Wen, C. Y.; Chen, K. H.; Lin, W. C.; Tsai, D. P. Near-Field Images of the AgO_x-Type Super-Resolution Near-Field Structure. *Appl. Phys. Lett.* **2001**, *78*, 685–687.
47. Kim, W.; Safonov, V. P.; Shalaev, V. M.; Armstrong, R. L. Fractals in Microcavities: Giant Coupled, Multiplicative Enhancement of Optical Responses. *Phys. Rev. Lett.* **1999**, *82*, 4811–4814.
48. Monti, O. L. A.; Fourkas, J. T.; Nesbitt, D. J. Diffraction-Limited Photogeneration and Characterization of Silver Nanoparticles. *J. Phys. Chem. B* **2004**, *108*, 1604–1612.
49. Raju, N. R. C.; Kumar, K. J. Photodissociation Effects on Pulsed Laser Deposited Silver Oxide Thin Films: Surface-Enhanced Resonance Raman Scattering. *J. Raman Spectrosc.* **2011**, *42*, 1505–1509.
50. Canamares, M. V.; Garcia-Ramos, J. V.; Sanchez-Cortes, S.; Castillejo, M.; Oujja, M. Comparative SERS Effectiveness of Silver Nanoparticles Prepared by Different Methods: A Study of the Enhancement Factor and the Interfacial Properties. *J. Colloid Interface Sci.* **2008**, *326*, 103–109.
51. Rakic, A. D.; Djurisic, A. B.; Elazar, J. M.; Majewski, M. L. Optical Properties of Metallic Films for Vertical-Cavity Optoelectronic Devices. *Appl. Opt.* **1998**, *37*, 5271–5283.
52. Kawata, S. *Near-Field Optics and Surface Plasmon Polaritons*; Springer: Berlin, 2001.
53. Aydin, K.; Ferry, V. E.; Briggs, R. M.; Atwater, H. A. Broadband Polarization-Independent Resonant Light Absorption Using Ultrathin Plasmonic Super Absorbers. *Nat. Commun.* **2011**, *2*, 517.
54. Sun, G.; Khurgin, J. B.; Soref, R. A. Practical Enhancement of Photoluminescence by Metal Nanoparticles. *Appl. Phys. Lett.* **2009**, *94*, 101103.
55. Cong, C. X.; Yu, T.; Sato, K.; Shang, J. Z.; Saito, R.; Dresselhaus, G. F.; Dresselhaus, M. S. Raman Characterization of ABA- and ABC-Stacked Trilayer Graphene. *ACS Nano* **2011**, *5*, 8760–8768.
56. Cong, C. X.; Yu, T.; Saito, R.; Dresselhaus, G. F.; Dresselhaus, M. S. Second-Order Overtone and Combination Raman Modes of Graphene Layers in the Range of 1690–2150 cm^{-1}. *ACS Nano* **2011**, *5*, 1600–1605.
57. Luo, Z. Q.; Yu, T.; Kim, K. J.; Ni, Z. H.; You, Y. M.; Lim, S.; Shen, Z. X.; Wang, S. Z.; Lin, J. Y. Thickness-Dependent Reversible Hydrogenation of Graphene Layers. *ACS Nano* **2009**, *3*, 1781–1788.
58. Baker, T. A.; Monti, O. L. A.; Nesbitt, D. J. Kinetic Studies of the Photogeneration of Silver Nanoparticles. *J. Phys. Chem. C* **2011**, *115*, 9861–9870.